

Article

Crystallographic Evidence of η^1 -Coordination of Bulky Aminopyridine in Halide-Containing Iron (II) Complexes

 Awal Noor 

Department of Basic Sciences, Preparatory Year Deanship, King Faisal University, Al-Hassa 31982, Saudi Arabia; anoor@kfu.edu.sa

Abstract: Reaction of N-(2,6-diisopropylphenyl)-[6-(2,4,6-triisopropylphenyl)-pyridine-2-yl]-amine (ApH) in equimolar ratio with anhydrous FeBr₂ and FeI₂ in tetrahydrofuran (THF) afforded, after workup in toluene, the first examples of mono(aminopyridine) Fe(II) complexes, [ApHFeBr(μ -Br)]₂ (**1**) and [ApHFeI₂(thf)] (**2**), respectively. X-ray analysis shows **1** to be dimeric, whereas compound **2** is monomeric. In both cases, aminopyridine ligands show rare η^1 -coordination to Fe through pyridine nitrogen atom. Compound **1** exhibits intramolecular N–H···Br hydrogen bonds [3.363 Å] with an N–H···Br angle of 158.84°. Hirshfeld surface and fingerprint plots identify the significant intermolecular interactions in the crystal network. Both compounds crystallized in the monoclinic space group. For compound **1**, C2/c, the cell parameters are: a = 25.5750(5) Å, b = 10.5150(5) Å, c = 18.9610(8) Å, β = 97.892(5)°, V = 5050.7(3) Å³, Z = 4. For compound **2**, P2₁/c, the cell parameters are: a = 10.3180(7) Å, b = 16.1080(10) Å, c = 18.6580(11) Å, β = 102.038(5)°, V = 3032.8(3) Å³, Z = 4.

Keywords: aminopyridine; iron; N-ligands; single crystal; X-ray analysis



Citation: Noor, A. Crystallographic Evidence of η^1 -Coordination of Bulky Aminopyridine in Halide-Containing Iron (II) Complexes. *Crystals* **2022**, *12*, 697. <https://doi.org/10.3390/cryst12050697>

Academic Editors: Paul R. Raithby, Assem Barakat, Ayman El-Faham and Saied Soliman

Received: 26 April 2022

Accepted: 12 May 2022

Published: 14 May 2022

Publisher's Note: MDPI stays neutral with regard to jurisdictional claims in published maps and institutional affiliations.



Copyright: © 2022 by the author. Licensee MDPI, Basel, Switzerland. This article is an open access article distributed under the terms and conditions of the Creative Commons Attribution (CC BY) license (<https://creativecommons.org/licenses/by/4.0/>).

1. Introduction

The coordination chemistry of 2-aminopyridines is a highly popular area of research mainly due to their easy accessibility as well as steric and electronic versatility [1,2]. The ligand class has shown rich coordination chemistry with predominantly chelating (common) and bridging coordination modes (Figure 1). In comparison, monodentate fashion of coordination to metal has rarely been observed. The η^1 -coordination via the pyridine nitrogen occurs particularly if the metal fragment is reluctant to accept six electrons resulting from π coordination [3]. On the other hand, η^1 -bonding via the weaker amine nitrogen is rather exceptional and may occur only if coordination at the pyridine N-donor site is not feasible for steric reasons.

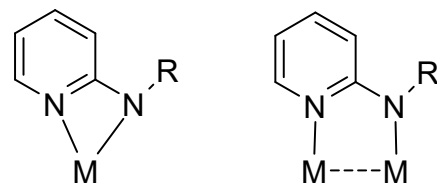


Figure 1. Chelating and bridging coordination modes of aminopyridinato ligands (R = alkyl, aryl or silyl; M = transition metal).

Since the introduction of bulky versions of these ligands in 2004, they have been successfully used to stabilize not only p-block and early transition metals but also lanthanides with good control of metal to ligand stoichiometry [2,4,5]. Surprisingly, their coordination chemistry with late transition metals has not been explored yet. Despite the fact that aminopyridines have been investigated for years, little is known about iron aminopyridinates [6]. Among late transition metals, the versatile coordination chemistry of iron in different oxidation states with a variety of chelating ligands has always attracted

chemists [7–9]. Iron commonly exists in +2 and +3 oxidation states [10,11]. It also rarely exists in +4 [12] and +5 [13] oxidation states. Due to our interest in stabilization and structural elucidation of transition metals in low or unusually low oxidation states [14–21], we opted to explore iron (II) complexes with varying halide ligands using saturated 2-aminopyridines. Saturated nitrogen ligands are known for their increased reducing power [22] and saturated α -aminopyridines of iron have been proven as efficient atom transfer radical transfer polymerization and isoprene polymerization catalysts [23,24]; however, their structural elucidation using single crystal analysis is not straightforward [25]. Here, we report the first examples of structurally characterized iron complexes with saturated 2-aminopyridines.

2. Materials and Methods

2.1. General Information

All manipulations were performed with the rigorous exclusion of oxygen and moisture in Schlenk-type glassware on a dual manifold Schlenk line or in an N₂-filled glove box (mBraun 120-G) with a high-capacity recirculator (<0.1 ppm O₂). Solvents were dried by distillation from sodium wire/benzophenone. Aminopyridine ligand was prepared according to the published procedure [4]. Elemental analyses (CHN) were determined using a Vario EL III instrument. X-ray crystal structure analyses were performed by using a STOE IPDSII equipped with an Oxford Cryostream low-temperature unit. Structure solution and refinement was accomplished using SIR97 [26], SHELXL2014 [27] and WinGX [28]. Data collection and cell refinement by X-Area-TOE. The single crystal was irradiated with Mo-K α at 133 K. The non-hydrogen atoms were refined with anisotropic thermal parameters. All hydrogen atoms except N-H (modelled using electron density) were added at calculated positions and refined using riding model. Crystallographic details are summarized in Table 1. CCDC-2168545 (1) and CCDC-2168544 (2) contain the supplementary crystallographic data for this paper. These data can be obtained free of charge at www.ccdc.cam.ac.uk/conts/retrieving.html (accessed on 6 May 2022) (or from the Cambridge Crystallographic Data Centre, 12 Union Road, Cambridge CB2 1EZ, UK; Fax: +44-1223-336-033; e-mail: deposit@ccdc.cam.ac.uk).

Table 1. Crystallographic data of the compounds 1 and 2.

Compound	1	2
CCDC number	2168545	2168544
Empirical formula	C ₅₀ H ₆₀ Br ₄ Fe ₂ N ₄	C ₂₉ H ₃₈ FeI ₂ N ₂ O
Formula weight	1148.36	740.26
crystal system	monoclinic	monoclinic
space group	C 2/c	P 2 ₁ /c
a [Å]	25.5750(5)	10.3180(7)
b [Å]	10.5150(5)	16.1080(10)
c [Å]	18.9610(8)	18.6580(11)
α [deg]		
β [deg]	97.892(5)	102.038(5)
γ [deg]		
V, [Å ³]	5050.7(3)	3032.8(3)
crystal size, [mm ³]	0.25 × 0.21 × 0.16	0.37 × 0.30 × 0.24
ρ_{calcd} , [g cm ⁻³]	1.510	1.621
μ , [mm ⁻¹] (Mo K α)	3.775	2.556
T, [K]	133(2)	133(2)
2 θ range, [deg]	3.22–53.18	3.37–53.13
No. of reflections unique	5052	6095
No. of reflections obs. [I > 2 σ (I)]	3014	4453
No. of parameters	281	326
wR ² (all data)	0.0816	0.1004
R value [I > 2 σ (I)]	0.0352	0.0375

2.2. Syntheses

Synthesis of **1**: ApH (358 mg, 1 mmol) was added to FeBr₂ (216 mg, 1 mmol) in tetrahydrofuran (THF) (50 mL) at room temperature and the resulting suspension was stirred overnight at 50°C. Solvent was evaporated and re-dissolved in toluene (20 mL). Solution was filtered and the volume was reduced to ca. 10 mL to afford orange crystals at room temperature. Yield: 220 mg (38.3%). Elemental analyses for C₅₀H₆₀Br₄Fe₂N₄ · H₂O: Calcd. C 51.49, H 5.36, N 4.80%; found C 51.57, H 5.39, N 4.71%.

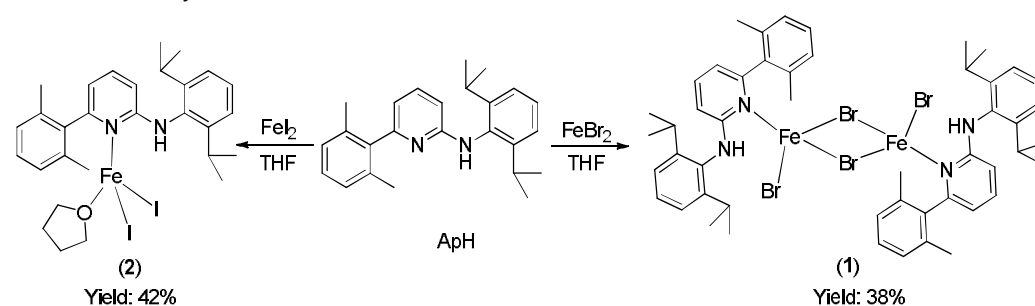
Synthesis of **2**: ApH (358 mg, 1 mmol) was added to FeI₂ (310 mg, 1 mmol) in THF (50 mL) at room temperature and the resulting brown-green solution was stirred overnight at 50°C. Solvent was evaporated and the material was re-dissolved in toluene (20 mL). Solution was filtered and the volume was reduced to ca. 10 mL to afford orange crystals at room temperature. Yield: 315 mg (42.5%). Elemental analyses for C₂₉H₃₈FeI₂N₂O: Calcd. C 47.05, H 5.17, N 3.78%; found C 46.55, H 5.05, N 3.57%.

2.3. Hirshfeld Surface Analysis

The Hirshfeld surfaces and 2D fingerprint plots were generated using Crystal Explorer 17.50 [29]. The X-ray single-crystal crystallographic information files were used as input files. The default setting used for Hirshfeld Surface/fingerprint generation in Crystal Explorer is as follows: property: none; resolution: High (standard). For fingerprint generation (di vs. de plot) we used: range: standard; filter: by elements and fingerprint filter options is both inside-outside elements including reciprocal contacts. The interactions with normalized contact distance in crystal structure shorter than the sum of the corresponding van der Waals radii of the atoms are highlighted by red spots and the longer contacts with the positive d_{norm} value are represented in blue colour.

3. Results

The two iron (II) compounds [ApHFeBr(μ-Br)]₂ (**1**) and [ApHFeI₂(thf)] (**2**), were prepared by reacting one equivalent of N-(2,6-diisopropylphenyl)-[6-(2,4,6-triisopropylphenyl)pyridine-2-yl]-amine (ApH) with anhydrous FeBr₂ and FeI₂, respectively in THF at room temperature (Scheme 1). After work up, orange crystals of paramagnetic **1** and **2** were isolated after couple of days from toluene solution at room temperature. Both compounds were characterized by single crystal X-ray analysis and the purity was further proved by elemental analysis.



Scheme 1. Synthesis of aminopyridine Fe complexes.

The molecular structure of **1** shows a centrosymmetric dinuclear mono(aminopyridine) iron bromide complex (Figure 2). Noteworthy is the rare η^1 -coordination of the aminopyridine ligand through pyridine nitrogen ($d(\text{N2-Fe1}) = 2.093(3) \text{ \AA}$) [30]. The coordination around each iron atom can be best described as distorted trigonal pyramidal and is completed by one N atom of the pyridine ring of the aminopyridine, and two bromide ligands. As expected, the Br-Fe bond for the bridging bromide ligand [Br1-Fe1 2.5260(8) Å] is longer than the terminal bromide ligand [Br2-Fe1 2.3985(8) Å] (Table 2). The long Fe...Fe distance of 3.439 Å rules out any possible metal-metal bonding interaction. It also exhibits intramolecular N-H...Br hydrogen bonds having an N...Br distance of 3.363 Å and an N-H...Br angle of 158.84°.

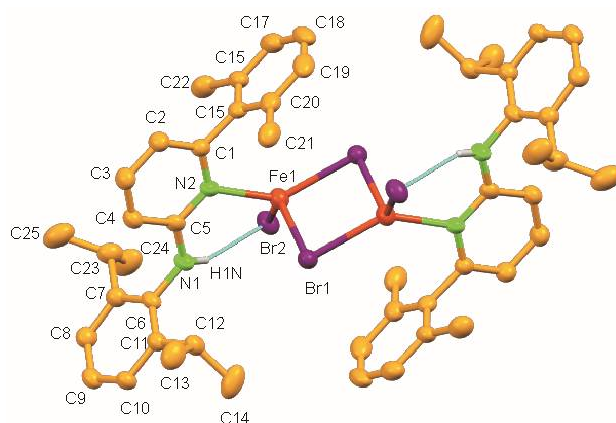


Figure 2. Molecular structure of **1**. Ellipsoids are set at 50 % probability; hydrogen atoms except N-H are omitted for clarity.

Table 2. Selected bond lengths (Å) and angles (°) of structures **1** and **2**.

Compound	Atoms	Bond Length	Atoms	Angles
1	Br1–Fe1	2.5260(8)	Fe1–Br1–Fe1	86.55(3)
	Br2–Fe1	2.3985(8)	N2–Fe1–Br2	104.84(10)
	Fe1–N2	2.093(3)	N2–Fe1–Br1	138.02(10)
			Br2–Fe1–Br1	103.62(3)
			N2–Fe1–Br1	98.07(10)
			Br2–Fe1–Br1	120.32(3)
			Br1–Fe1–Br1A	93.45(2)
			N2–C5–N1	117.3(3)
2	I1–Fe1	2.6245(7)	O1–Fe1–N3	123.45(13)
	I2–Fe1	2.6024(7)	O1–Fe1–I2	100.82(9)
	Fe1–O1	2.032(3)	N3–Fe1–I2	108.21(9)
	Fe1–N3	2.080(3)	O1–Fe1–I1	105.87(9)
			N3–Fe1–I1	106.25(0)
			I2–Fe1–I1	112.22(3)
		C5–N1–C6	123.4(4)	

Hirshfeld surface analyses were used to get insights into the detailed information about the strength of intermolecular interactions. The interactions with normalized contact distance in crystal structure shorter than the sum of the corresponding van der Waals radii of the atoms, are highlighted by red spots and the longer contacts with the positive d_{norm} value are represented in blue colour (Figure 3). The significant intermolecular interactions are mapped in Figure 4. On the Hirshfeld surfaces, the H \cdots H interactions appear as the largest region (76.4%) of the fingerprint plot. The C–H \cdots π interactions give rise to a pair of characteristic wings in the fingerprint plot decomposed into C \cdots H/H \cdots C contacts contributing 12.3%. The pair of sharp spikes represent the Br \cdots H/H \cdots Br contacts with a contribution of 10 % due to the intermolecular C–H \cdots Br hydrogen bonding. The C \cdots C π interactions are found to be negligible (1.3%).

The molecular structure of **2** shows a monomeric mono(aminopyridine) iron iodide complex (Figure 5). The coordination around each iron atom can be best described as distorted tetrahedral and is completed by one N atom of the pyridine ring of the aminopyridine, two iodides and an O atom of the tetrahydrofuran ligand. Although the aminopyridine ligand is η^1 -coordinated ($d(\text{N3}–\text{Fe1}) = 2.080(3)$ Å), no intramolecular hydrogen bonding has been observed. The formation of monomeric structure and lack of hydrogen bonding may be attributed to the larger size and the electro-positivity of the iodide ligand. This is also evident by the comparatively wider C–N–C bond angle [$\text{C5}–\text{N1}–\text{C6}$ 123.4(4)°] of the aminopyridine ligand in **2** than in **1** [$\text{N2}–\text{C5}–\text{N1}$ 117.3(3)°] (Table 2).

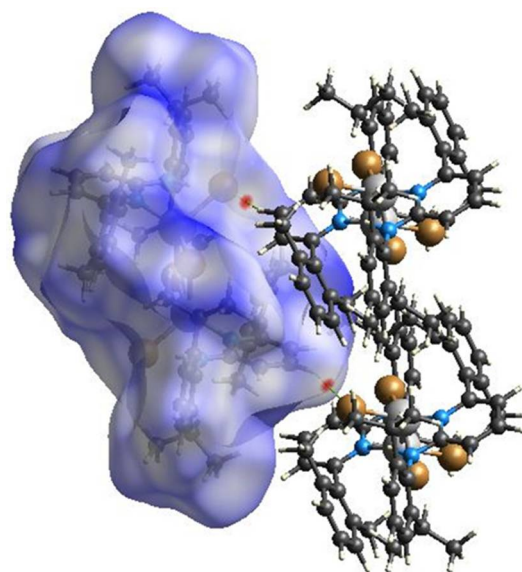


Figure 3. View of the three-dimensional Hirshfeld surface of **1** plotted over d_{norm} in the range -0.0639 to 1.8424 .

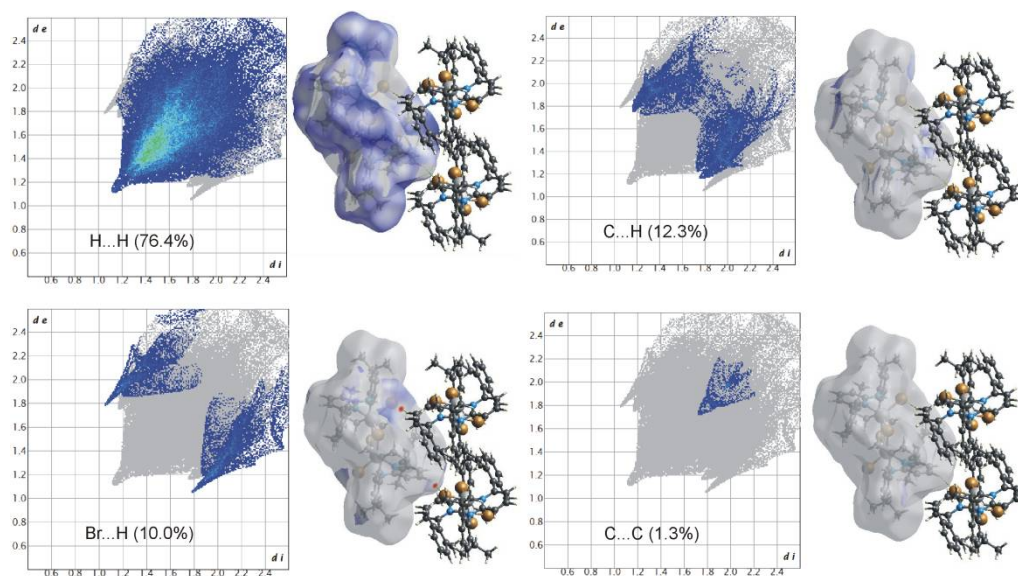


Figure 4. Two-dimensional fingerprint plots for all intermolecular contacts in **1**. The percentage of contribution is specified for each contact.

Hirshfeld surface analyses show that although the fingerprint profiles are still dominated by $\text{H}\cdots\text{H}$ contacts (72.4%), the contributions due to the intermolecular $\text{C}\text{-H}\cdots\text{I}$ hydrogen bonding are the maximum that have been observed (Figures 6 and 7). The $\text{I}\cdots\text{H}/\text{H}\cdots\text{I}$ interactions contribute 16.5%, and due to the intermolecular $\text{C}\text{-H}\cdots\text{I}$ hydrogen bonding, these contacts appear as sharp spike to the fingerprint profile. Other major contributions are due to the $\text{C}\text{-H}\cdots\pi$ interactions (10.7%) forming a pair of characteristic wings.

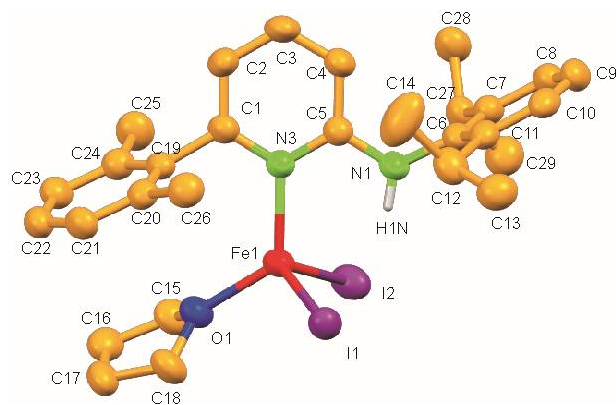


Figure 5. Molecular structure of **2**. Ellipsoids are set at 50% probability; hydrogen atoms except N-H are omitted for clarity.

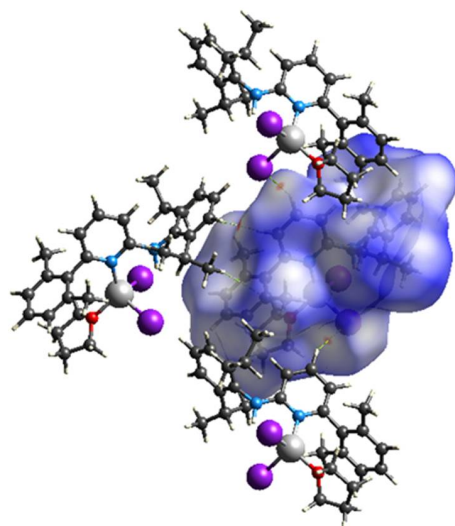


Figure 6. View of the three-dimensional Hirshfeld surface of **2** plotted over d_{norm} in the range -0.0888 to 1.3946 .

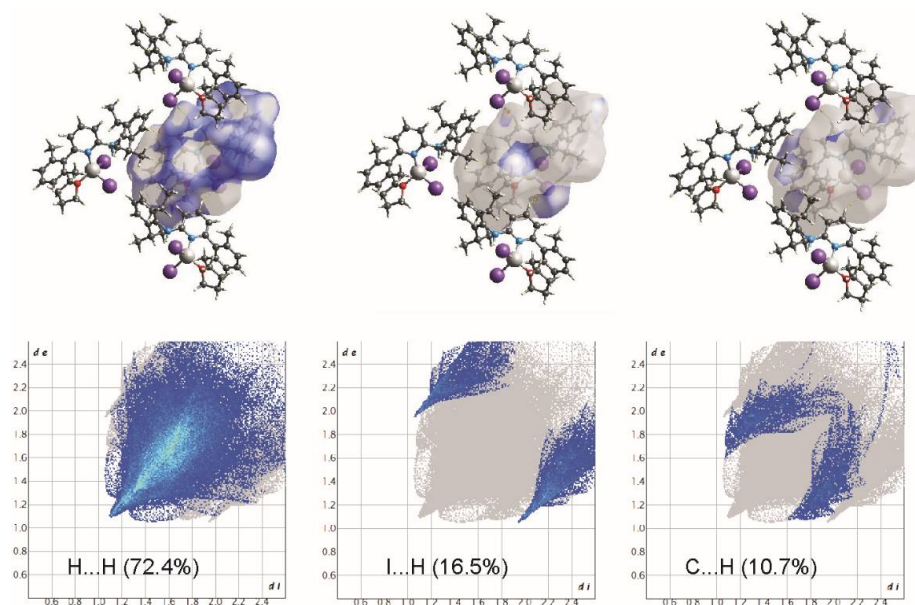


Figure 7. Two-dimensional fingerprint plots for all intermolecular contacts in **2**. The percentage of contribution is specified for each contact.

4. Conclusions

The first examples of structurally characterized iron (II) halide complexes of saturated 2-aminopyridine are reported here. The coordinated aminopyridine ligand adopts rare η^1 -coordination through a pyridine nitrogen atom instead of the chelating mode known for the majority of aminopyridine complexes. The formation of dimeric or monomeric structures could be attributed to the varying sizes of coordinated halide ligands. The dimeric compound **1** exhibits intramolecular hydrogen bonding. Hirshfeld surface analyses also identified significant intermolecular interactions in the crystal network for both the complexes.

Funding: This work was supported by the Deanship of Scientific Research, King Faisal University, Saudi Arabia (Grant Number NA000182).

Institutional Review Board Statement: Not applicable.

Informed Consent Statement: Not applicable.

Data Availability Statement: Supplementary crystallographic data can be obtained online free of charge via <http://www.ccdc.cam.ac.uk/conts/retrieving.html> (accessed on 6 May 2022).

Acknowledgments: This work was supported by the Deanship of Scientific Research, King Faisal University, Saudi Arabia (Grant Number NA000182). The author extends his thanks to Rhett Kempe from University of Bayreuth, Germany for the access to the laboratory facilities and useful discussions.

Conflicts of Interest: The author declares no conflict of interest.

References

1. Kempe, R. The strained η^2 -N_{Amido}-N_{Pyridine} coordination of aminopyridinato ligands. *Eur. J. Inorg. Chem.* **2003**, *2003*, 791–803. [[CrossRef](#)]
2. Noor, A. Coordination chemistry of bulky aminopyridinates with main group and transition metals. *Top. Curr. Chem.* **2021**, *379*, 6. [[CrossRef](#)] [[PubMed](#)]
3. Scott, N.M.; Schareina, T.; Tok, O.; Kempe, R. Lithium and Potassium Amides of Sterically Demanding Aminopyridines. *Eur. J. Inorg. Chem.* **2004**, *2004*, 3297–3304. [[CrossRef](#)]
4. Xu, X.; James, S.L.; Mingos, D.M.P.; White, A.J.P.; Williams, D.J. Platinum(II) phosphine and orotate complexes with aminopyridine co-ligands, and their molecular recognition via hydrogen bonding. *J. Chem. Soc. Dalton Trans.* **2000**, *29*, 3783–3790. [[CrossRef](#)]
5. Kempe, R. Rare Earth Polymerization Catalysts Supported by Bulky Aminopyridinato Ligands. *Z. Anorg. Allg. Chem.* **2010**, *636*, 2135–2147. [[CrossRef](#)]
6. Glatz, G.; Demeshko, S.; Motz, G.; Kempe, R. First Row Transition Metal Aminopyridinates—The Missing Complexes. *Eur. J. Inorg. Chem.* **2009**, *2009*, 1385–1392. [[CrossRef](#)]
7. Chen, M.S.; White, M.C. A Predictably Selective Aliphatic C–H Oxidation Reaction for Complex Molecule Synthesis. *Science* **2007**, *318*, 783–787. [[CrossRef](#)]
8. Nielsen, A.; Larsen, F.B.; Bond, A.D.; McKenzie, C.J. Regiospecific Ligand Oxygenation in Iron Complexes of a Carboxylate-Containing Ligand Mediated by a Proposed Fe^V-Oxo Species. *Angew. Chem. Int. Ed.* **2006**, *118*, 1632–1636. [[CrossRef](#)]
9. Costas, M.; Chen, K.; Que, L., Jr. Biomimetic nonheme iron catalysts for alkane hydroxylation. *Coord. Chem. Rev.* **2000**, *200–202*, 517–544. [[CrossRef](#)]
10. Sundaresan, S.; Eppelsheimer, J.; Carrella, L.M.; Rentschler, E. Three Novel Thiazole-Arm Containing 1,3,4-Oxadiazole-Based [HS-HS] Fe(II) Dinuclear Complexes. *Crystals* **2022**, *12*, 404. [[CrossRef](#)]
11. Sundaresan, S.; Kühne, I.A.; Kelly, C.T.; Barker, A.; Salley, D.; Müller-Bunz, H.; Powell, A.K.; Morgan, G.G. Anion Influence on Spin State in Two Novel Fe(III) Compounds: [Fe(5F-sal₂333)]X. *Crystals* **2019**, *9*, 19. [[CrossRef](#)]
12. Prakash, O.; Chábera, P.; Rosemann, N.W.; Huang, P.; Häggström, L.; Ericsson, T.; Strand, D.; Persson, P.; Bendix, J.; Lomoth, R.; et al. A Stable Homoleptic Organometallic Iron(IV) Complex. *Chem. Eur. J.* **2020**, *26*, 12728–12732. [[CrossRef](#)] [[PubMed](#)]
13. Ghosh, M.; Singh, K.K.; Panda, C.; Weitz, A.; Hendrich, M.P.; Collins, T.J.; Dhar, B.B.; Sen Gupta, S. Formation of a Room Temperature Stable Fe^V(O) Complex: Reactivity Toward Unactivated C–H Bonds. *J. Am. Chem. Soc.* **2014**, *136*, 9524–9527. [[CrossRef](#)] [[PubMed](#)]
14. Noor, A.; Wagner, F.R.; Kempe, R. Metal–metal distances at the limit: A coordination compound with an ultrashort chromium–chromium bond. *Angew. Chem. Int. Ed.* **2008**, *47*, 7246–7249. [[CrossRef](#)] [[PubMed](#)]
15. Noor, A.; Glatz, G.; Müller, R.; Kaupp, M.; Demeshko, S.; Kempe, R. Carboalumination of a chromium–chromium quintuple bond. *Nat. Chem.* **2009**, *1*, 322–325. [[CrossRef](#)] [[PubMed](#)]

16. Noor, A.; Qayyum, S.; Schwarz, S.; Dietel, T.; Kempe, R. Formation of a dimeric tungsten(I) complex via C-H activation. *Dalton Trans.* **2020**, *49*, 1992–1996. [[CrossRef](#)] [[PubMed](#)]
17. Noor, A.; Bauer, T.; Todorova, T.K.; Weber, B.; Gagliardi, L.; Kempe, R. The ligand-based quintuple bond-shortening concept and some of its limitations. *Chem. Eur. J.* **2013**, *19*, 9825–9832. [[CrossRef](#)]
18. Noor, A.; Glatz, G.; Müller, R.; Kaupp, M.; Demeshko, S.; Kempe, R. Metal–metal distances at the limit: Cr–Cr 1.73 Å—The importance of the ligand and its fine tuning. *Z. Anorg. Allg. Chem.* **2009**, *635*, 119–1152. [[CrossRef](#)]
19. Wagner, F.R.; Noor, A.; Kempe, R. Ultrashort metal–metal distances and extreme bond orders. *Nat. Chem.* **2009**, *1*, 529–536. [[CrossRef](#)]
20. Noor, A.; Kempe, R. The shortest metal–metal bond. *Chem. Rec.* **2010**, *10*, 413–416. [[CrossRef](#)]
21. Noor, A.; Kempe, R. M5M—Key compounds of the research field metal–metal quintuple bonding. *Inorg. Chim. Acta* **2014**, *424*, 75–82. [[CrossRef](#)]
22. Xia, J.; Matyjaszewski, K. Controlled/“Living” Radical Polymerization. Atom Transfer Radical Polymerization Using Multidentate Amine Ligands. *Macromolecules* **1997**, *30*, 7697–7700. [[CrossRef](#)]
23. Thierer, L.M.; Jenny, S.E.; Shastri, V.; Donley, M.R.; Round, L.M.; Piro, N.A.; Kassel, W.S.; Brown, C.L.; Dudley, T.J.; Zubris, D.L. Amino pyridine iron(II) complexes: Characterization and catalytic application for atom transfer radical polymerization and catalytic chain transfer. *J. Organomet. Chem.* **2020**, *924*, 121456. [[CrossRef](#)]
24. Jing, C.; Wang, L.; Mahmood, Q.; Zhao, M.; Zhu, G.; Zhang, X.; Wang, X.; Wang, Q. Synthesis and characterization of aminopyridine iron(II) chloride catalysts for isoprene polymerization: Sterically controlled monomer enchainment. *Dalton Trans.* **2019**, *48*, 7862–7874. [[CrossRef](#)] [[PubMed](#)]
25. Gibson, V.C.; O’Reilly, R.K.; Wass, D.F.; White, A.J.P.; Williams, D.J. Iron complexes bearing iminopyridine and aminopyridineli-gands as catalysts for atom transfer radical polymerization. *Dalton Trans.* **2003**, *32*, 2824–2830. [[CrossRef](#)]
26. Altomare, A.; Burla, M.C.; Camalli, M.; Cascarano, G.L.; Giacovazzo, C.; Guagliardi, A.; Moliterni, A.G.G.; Polidori, G.; Spagna, R. SIR 97: A new tool for crystal determination and refinement. *J. Appl. Crystallogr.* **1999**, *32*, 115–119. [[CrossRef](#)]
27. Sheldrick, G.M. A short history of SHELX. *Acta Crystallogr. Sect. A* **2008**, *64*, 112–122. [[CrossRef](#)] [[PubMed](#)]
28. Farrugia, L.J. WinGX Suite for small-molecule single-crystal crystallography. *J. Appl. Crystallogr.* **1999**, *32*, 837–838. [[CrossRef](#)]
29. Turner, M.J.; McKinnon, J.J.; Wolff, S.K.; Grimwood, D.J.; Spackman, P.R.; Jayatilaka, D.; Spackman, M.A. *Crystal Explorer 17*; University of Western Australia: Perth, WA, Australia, 2017.
30. Ayuso, A.E.; Noor, A.; Irrgang, T.; Glatz, G.; Kempe, R. Crystal structure of (2,6-diisopropyl-phenyl)-(6-(2,6-dimethyl-phenyl)-pyridin-2-yl)-amine-(2,6-diisopropyl-phenyl)-(6-(2,6-dimethyl-phenyl)-pyridin-2-yl)-amido-lithium, Li(C₂₅H₂₉N₂)(C₂₅H₃₀N₂). *Z. Kristallogr. NCS* **2007**, *222*, 281–283. [[CrossRef](#)]